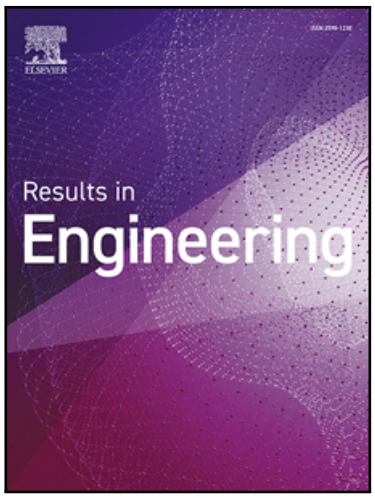

Optimization, Characterization, and DFT Study of Activated-Biochar from Lignocellulosic Biomass for Fluoroquinolone Antibiotic Adsorption

Kawtar Ezzahi , Imad Rabichi , Hasna Befenzi , Eric Record , Taoufiq Bouzid , Abdelghani Yaacoubi , Abdelaziz Baçaoui , Youssef Habibi , Loubna El Fels

PII: S2590-1230(25)02609-X
DOI: https://doi.org/10.1016/j.rineng.2025.106540
Reference: RINENG 106540

To appear in: *Results in Engineering*

Received date: 23 June 2025
Revised date: 21 July 2025
Accepted date: 30 July 2025

Please cite this article as: Kawtar Ezzahi , Imad Rabichi , Hasna Befenzi , Eric Record , Taoufiq Bouzid , Abdelghani Yaacoubi , Abdelaziz Baçaoui , Youssef Habibi , Loubna El Fels , Optimization, Characterization, and DFT Study of Activated-Biochar from Lignocellulosic Biomass for Fluoroquinolone Antibiotic Adsorption, *Results in Engineering* (2025), doi: https://doi.org/10.1016/j.rineng.2025.106540

Highlights

- KOH-activated carbon and BC showed BET surface areas of 829.76 m^2/g and 258.72 m^2/g, respectively.
- AC demonstrated strong potential for fluoroquinolone removal in wastewater treatment.
- Adsorption capacity reached up to 147.68 mg/g for ciprofloxacin.
- Competitive sorption affinities followed the order: CIP> ENR > LEV
- DFT study revealed fluoroquinolone antibiotics adsorption mechanisms at the molecular level.

Optimization, Characterization, and DFT Study of Activated-Biochar from Lignocellulosic Biomass for Fluoroquinolone Antibiotic Adsorption

Kawtar Ezzahi[a], Imad Rabichi[b,a], Hasna Befenzi[a], Eric Record[C*], Taoufiq Bouzid[d], Abdelghani Yaacoubi[b], Abdelaziz Baçaoui[b], Youssef Habibi[e], Loubna El Fels[a,e*]

[a] Cadi Ayyad University, Faculty of Sciences Semlalai, Laboratory of Water Sciences, Microbial Biotechnologies, and Natural Resources Sustainability (AQUABIOTECH), Unit of Microbial Biotechnologies, Agrosciences, and Environment (BIOMAGE)-CNRST Labeled Research Unit N°4, PO Box 2390, Marrakech 40000, Morocco

[b] Laboratory of Applied Chemistry and Biomass, Faculty of Sciences Semlalia, Cadi Ayyad University, Marrakech 40000, Morocco

[C] INRAE, Aix Marseille Univ, BBF, Biodiversité et Biotechnologie Fongiques, Marseille, France
Polytechnic (UM6P), Lot 660, Hay Moulay Rachid, Benguerir, 43150, Morocco

[d] Laboratoire de chimie analytique et moléculaire, Cadi Ayyad University, Faculty polydisciplinaire, Safi, Morocco

e Sustainable Materials Research Center (SUSMAT-RC), University Mohamed VI Polytechnic (UM6P), Lot 660, Hay Moulay Rachid, Benguerir, 43150, Morocco

Corresponding author:

Loubna EL FELS: loubna.elfels@uca.ac.ma

Eric Record: eric.record@inrae.fr

Abstract

The presence of fluoroquinolone antibiotics in water bodies poses a significant environmental concern due to their persistence and potential ecological risks. This study explores the adsorption efficiency of BC and AC derived from lignocellulosic biomass for the removal of ciprofloxacin (CIP), levofloxacin (LEV), and enrofloxacin (ENR) from aqueous solutions. The results revealed that KOH activation significantly enhanced the surface area of AC (829.76 m^2/g), compared to BC (258.72 m^2/g), leading to a higher adsorption capacity. Adsorption kinetics were most accurately represented by the pseudo-second-order model, indicating that chemisorption is the primary mechanism in the adsorption process. Equilibrium data were fitted to both the Langmuir and Freundlich isotherm models, with the Langmuir model yielding the best fit, confirming monolayer adsorption. The maximum adsorption capacities (q_m) obtained for AC were 147.68 mg/g for CIP, 134.29 mg/g for LEV, and 128.53 mg/g for ENR, highlighting the superior adsorption potential of AC compared to BC. Thermodynamic research found that the adsorption process was spontaneous and endothermic, with rising temperature favoring adsorption. Furthermore, the Elovich model provided additional insights into the heterogeneous nature of the adsorption sites and the strong affinity between the antibiotics and the adsorbent surface. The results demonstrate the high efficiency of AC in removing pharmaceutical pollutants, emphasizing its potential for application in wastewater treatment and environmental remediation.

Keywords: Adsorption, Antibiotic, Biochar, DFT, Fluoroquinolones, kinetics.

1. Introduction

Water is an essential resource for sustaining life, driving economic development, and preserving ecological integrity. However, the growing contamination of aquatic environments by a wide range of pollutants poses serious threats to both environmental and human health [1]. Among these contaminants, antibiotics have garnered increasing attention due to their widespread use in human and veterinary medicine, as well as their persistence in the environment [2]. These pharmaceuticals can disrupt aquatic ecosystems and contribute to the emergence and spread of antimicrobial resistance, a pressing global health issue [3].

Fluoroquinolones are a commonly used class of antibiotics with broad-spectrum antibacterial properties. However, their widespread use and persistence in the environment result in their frequent occurrence and detection in wastewater, surface water, and even drinking water, which raises serious concerns about ecological health and antimicrobial

resistance. For example, research conducted in Fez, Morocco, discovered that surface water contained 438–1058 ng.L^{-1} of ciprofloxacin [4]. According to Gothwal & Shashidhar, the Musi River in India has elevated levels of ciprofloxacin, ofloxacin, norfloxacin, and enrofloxacin [5]. Arun et al. (2020) discovered fluoroquinolones in soil and sludge in Chennai, India, at levels of around 20 μg/g and 26 μg/g, respectively [6]. Ciprofloxacin, levofloxacin, and enrofloxacin were specifically selected for this study due to their widespread use in human and veterinary medicine [7], frequent detection in various aquatic environments [8,9], and differing chemical structures and degrees of degradation resistance [10,11], which together provide a representative basis for evaluating adsorbent performance. Unfortunately, conventional wastewater treatment processes are unable to completely remove fluoroquinolones, making it essential to investigate more effective and sustainable methods for their removal. Even at trace concentrations, the presence of fluoroquinolones in the environment can lead to serious ecological consequences, including the disruption of microbial communities and the promotion of antibiotic-resistant bacteria [9]. Conventional wastewater treatment methods, such as biological processes and chemical treatments, often fall short in effectively removing these persistent contaminants from water sources. Consequently, there is a growing need for more efficient and sustainable treatment technologies that can overcome the limitations of traditional methods [12].

Several methods have been employed to degrade fluoroquinolones, including advanced oxidation processes [13] and fungal bioremediation [14]. However, these approaches often face challenges, including the generation of toxic by-products [15] and the persistence of antimicrobial activity in the treated water [16]. In addition to these, alternative techniques such as membrane technology [10], adsorption [17], and coagulation-flocculation [18] have been explored, each with its unique advantages and challenges in the removal of fluoroquinolones.

Among these, adsorption stands out due to its operational simplicity, cost-effectiveness, and high efficiency in removing a broad spectrum of pollutants [19,20]. Numerous studies have shown that adsorption is highly effective for removing organic pollutants, including synthetic dyes and antibiotics, using low-cost materials such as coconut-shell-derived activated carbon and carbon nanotubes [21,22]. The effectiveness of adsorption is heavily influenced by the characteristics of the adsorbent material, which plays a critical role in determining its capacity for contaminant removal. Various materials have been investigated as potential adsorbents, including graphene oxide [23], nano-hydroxyapatite [24], Clay-based

nanomaterials [25], metal–organic frameworks [26], and multi-walled carbon nanotubes [27]. However, the high cost of these materials, along with the toxic and flammable nature of some of their precursors, limits their practical application [28]. In recent years, biochar derived from various biomass sources has emerged as a crucial material for the removal of antibiotics from the environment.

Biochar has proven to be a highly effective adsorbent for the removal of antibiotics, particularly due to its extensive surface area, porous structure, and robust interaction with organic contaminants [17]. These properties facilitate the efficient adsorption of substances like fluoroquinolones through various mechanisms, including hydrogen bonding, electrostatic interactions, π–π stacking, and hydrophobic effects, each of which plays a crucial role in the removal process. Furthermore, biochar is often modified with acids, bases, and oxidants to enhance the physicochemical features of its surface [29]. This modification further enhances its adsorption capacity, making biochar an even more efficient and versatile material for fluoroquinolones removal. In support of this, Genç and Dogan (2015) reported that activated carbon could achieve up to 87% removal of ciprofloxacin from aqueous solutions [30]. Similarly, Li et al. highlighted the effectiveness of biochar as a reliable adsorbent for antibiotic removal, underscoring its potential for efficient fluoroquinolone adsorption [31].

Complementing experimental investigations, theoretical and computational modeling have become an indispensable tool for understanding the fundamental mechanisms of adsorption at the molecular level. Recent advancements in Density Functional Theory (DFT) and related methods allow researchers to predict the structural, electronic, and energetic interactions between adsorbents and contaminants. For instance, theoretical studies have been successfully applied to model the adsorption of various molecules on novel surfaces, predict binding energies, and analyze the electronic changes that govern the adsorption process [32,33]. This computational approach provides critical insights into non-covalent interactions, charge transfer, and molecular stability, which are essential for designing more effective materials, as demonstrated in fields ranging from pharmaceuticals to materials science [34,35]. By integrating these theoretical analyses, researchers can bridge the gap between observed performance and the underlying molecular phenomena, accelerating the development of next-generation adsorbents.

Key parameters such as surface area, pore size, and pH of the adsorbent significantly influence the adsorption performance of these materials for fluoroquinolones. Understanding

these factors is critical for optimizing adsorption-based water treatment processes and enhancing the efficiency of antibiotic removal from contaminated water [36].

This study examines the potential of BC and AC, derived from olive mill solid waste (OMSW), for removing fluoroquinolones (levofloxacin, ciprofloxacin, and enrofloxacin) from polluted water. To enhance their adsorption capacity, biochar was chemically activated with potassium hydroxide (KOH) to produce activated carbon. Both BC and AC were extensively characterized using scanning electron microscopy (SEM) and Fourier transform infrared spectroscopy (FTIR). The adsorption efficiency of these materials was evaluated through various adsorption models, including pseudo-first-order, pseudo-second-order, and Elovich models, along with isotherm models such as Freundlich and Langmuir. Furthermore, the interaction between the adsorbents and fluoroquinolones was analyzed using DFT to better understand the underlying adsorption mechanisms.

To the best of our knowledge, this is the first study to report the application of OMSW-derived biochar for fluoroquinolone removal from water. By utilizing a sustainable biomass source, this research offers a novel and environmentally friendly solution to address pharmaceutical contamination in water systems. The findings highlight the potential of BC and AC as effective, cost-efficient materials for water purification, contributing valuable insights to the development of wastewater treatment technologies and the mitigation of pharmaceutical pollution.

2. Materials and Methods

2.1. Materials and chemicals

Olive Mill Solid Waste was collected from the Marrakech province, Morocco, and used as the raw material for biochar preparation. Potassium hydroxide (KOH, ≥85%) was obtained from Sigma-Aldrich and used as an activating agent. Enrofloxacin (ENR) ($C_{19}H_{22}FN_3O_3$, purity >99.0%), Levofloxacin (LEV) ($C_{18}H_{20}FN_3O_4$, purity >99.0%), and Ciprofloxacin (CIP) ($C_{17}H_{18}FN_3O_3$, purity >99.0%) were purchased from Sigma-Aldrich (USA). Stock solutions of these pharmaceuticals were prepared in distilled water and stored at 4°C.

2.2. Biochar Preparation

Biochar was produced from OMSW using pyrolysis in a cylindrical reactor under controlled oxygen conditions, following the procedure outlined in Rabichi et al.[37]. A total of 35 kg of OMSW was processed in a nitrogen environment. The pyrolysis conditions were

optimized based on key factors, including residence time, temperature, and heating rate. A pyrolysis temperature of 585 ± 5°C, a residence duration of 90 minutes, and a heating rate of 10°C/min were found to be the ideal parameters. After the pyrolysis process, the resulting biochar was thoroughly washed with distilled water to remove any residual impurities, ensuring high material purity. This washing step is essential to prevent any contaminants from interfering with subsequent adsorption experiments.

2.3. Biochar Activation

To improve the adsorption capacity of the biochar, a chemical activation process was performed using KOH, following the methodology described in Rabichi et al. [37]. The activation process involves impregnating the biochar with KOH in a 1:1 mass ratio, stirring the mixture for 2 hours at 60°C, and heating it to 110°C to facilitate water evaporation. The biochar was then subjected to thermal activation at 700 ± 2°C for 30 minutes under a nitrogen flow (100 mL/min) to ensure an inert atmosphere and prevent oxidation. This activation process developed the biochar's porous structure, which enhances its surface area and adsorption efficiency. After activation, the biochar was washed with distilled water until it reached a neutral pH (pH=6), then dried and stored for subsequent use in adsorption experiments.

2.4. Analytical Methods

The elemental composition of carbon (C), hydrogen (H), nitrogen (N), and sulfur (S) in the biochar samples was analyzed using a Euro EA CHNSO Elemental Analyzer. Ash content was determined by gradually heating the samples from ambient temperature to 750°C at a controlled rate of 5°C/min, maintaining this temperature for 6 hours, and then cooling to 105°C, following ASTM Standard D1762-84. The volatile matter content was measured by heating pre-dried biochar samples at 105°C in covered crucibles within a furnace preheated to 950°C, as per ASTM Standard D1762-84.

Fourier Transform Infrared Spectroscopy (FTIR) was conducted using a Bruker VERTEX 70 spectrometer to identify functional groups in biochar and activated carbon samples. Spectra were recorded within the 400–4000 cm^{-1} range using the potassium bromide (KBr) pellet technique. The materials' surface morphology and elemental composition were examined through field emission scanning electron microscopy (FESEM, VEGA3 LMU), coupled with an energy-dispersive X-ray (EDX) analyzer.

3. Results and discussion

3.1. Biomass characterization

Thermogravimetric analyses (TGA/DTA) carried out under an inert atmosphere (N_2) were used to evaluate the pyrolytic behavior of the selected precursors (**Fig.1**). Biomass combustion can be divided into three phases. During the first stage, the adsorbed water is evaporated, and the organic matter decomposes into lower molar mass intermediates, releasing volatile gaseous compounds [38]. The intermediates then decompose further to form other volatile species, tar, and char during the second phase.

The thermal decomposition of olive pomace occurs in three distinct stages. The first stage, known as the dehydration phase, takes place at low temperatures, from room temperature up to approximately 115 °C, and is primarily characterized by the loss of moisture in various forms, resulting in a weight loss of about 3% as shown by the TGA curve. The second stage, or rapid weight loss phase, spans from 160 to 350 °C and corresponds to the significant thermal degradation of organic components, particularly hemicellulose and cellulose, as well as the distillation of tars. During this phase, a substantial weight loss of around 60% is observed. The DTA curve shows two distinct peaks at 270 and 320 °C, associated with the decomposition of hemicellulose and cellulose, respectively. The final stage, the slow weight loss phase, occurs above 400 °C and extends up to 800 °C, reflecting the gradual degradation of lignin. This slow breakdown promotes the recombination of chemical structures, leading to the formation of a stable carbonaceous matrix a critical step in the production of activated carbon and biochar [39].

3.2. Adsorbents characterization

3.2.1. Features and XRD of Biochar and activated carbon

The FTIR spectra of BC and AC revealed significant differences in their surface functionalities, reflecting the structural modifications induced by pyrolysis and chemical activation. As shown in **Fig. 2**, a broad absorption around 3400 cm^{-1} is attributed to O–H stretching from hydroxyl-containing groups and adsorbed water, confirming the hydrophilic nature of BC [40]. Weak absorption bands in the 3000–2800 cm^{-1} range correspond to the symmetric and asymmetric stretching vibrations of aliphatic C–H groups. A pronounced peak around 2370 cm^{-1} is assigned to O–C=O stretching, suggesting ester formation due to interactions between carboxylic and phenolic groups in the precursor. Notably, the peak around 1740 cm^{-1}, which intensifies with higher KOH activation, is associated with C=O

stretching from ester or carboxylic acid group, indicating an increased concentration of oxygenated functionalities. This increase in oxygenated functional groups is primarily due to the KOH activation process, which promotes the formation of surface oxygen functionalities such as carboxyl, carbonyl, and hydroxyl groups by etching the carbon matrix and introducing defects [41–43]. Thorough washing with distilled water ensures the removal of residual activating agents, minimizing contamination. Similar observations have been reported in the literature, confirming that chemical activation effectively enhances surface oxygen content, thereby improving adsorptive interactions with polar pollutants [44,45]. The spectral region between 1720–1018 cm^{-1} exhibits typical bands of carbonyl groups and aromatic C=C stretching, suggesting the presence of lignin- and cellulose-derived structures. These findings indicate a progressive reduction in functional group diversity after activation, with AC retaining mainly C=O, C–C, and hydroxyl groups as confirmed by CHN elemental analysis. The enrichment of oxygen-containing groups upon activation contributes to enhanced adsorption properties, making both materials promising for pollutant removal applications [46,47].

X-ray diffraction analysis was conducted to evaluate the structural order of the samples, as illustrated in **Fig. 3**. The lack of sharp diffraction peaks indicates that both activated carbon and biochar possess predominantly amorphous structures. However, some broad peaks were identified around $2\theta = 24.43°$, 43.57°, and 44.69°, which correspond to the (002), (100), and (101) crystallographic planes, respectively. These reflections are typically associated with the stacking and lateral dimensions of aromatic carbon layers, suggesting the presence of disordered graphitic domains within the carbon matrix [48].

3.2.2. Proximate analysis

The proximate analysis of BC and AC was conducted to evaluate their potential for adsorption applications, particularly on key components such as fixed carbon, volatile matter, and ash content. These parameters are critical in determining the material's stability, adsorptive capacity, and overall effectiveness in environmental remediation [49]. Biochar demonstrated a fixed carbon content of 82.15%, indicating a significant amount of carbonaceous material, essential for adsorptive interactions. In comparison, activated carbon exhibited a notably higher fixed carbon content of 93.70%. This factor enhances its adsorption performance due to more available active sites for adsorbing organic contaminants [50]. The low ash content of 4.92 % for BC, and 6.06% for AC in both adsorbents suggests minimal inorganic impurities. Meanwhile, the volatile matter was significantly reduced in AC (0.24%)

compared to BC (12.93%), which enhances the thermal stability and adsorption efficiency of the material. These results suggest that AC, with its lower volatile matter and higher fixed carbon content, exhibits superior adsorption potential due to its enhanced porosity and stability [37,51,52].

3.2.3. Elemental analysis

Significant compositional changes were observed between BC and BC following KOH activation, particularly in carbon, oxygen, and hydrogen content. Biochar exhibited a high carbon content (90.12%), reflecting a well-structured carbonaceous matrix with minimal oxidation. After KOH activation, carbon content slightly decreased to 85.22%, indicating partial oxidation and the formation of new functional groups. These findings are consistent with previous findings, such as the study on bamboo-derived biochar, where carbon content dropped from 90% to 80.49% following KOH treatment, attributed to the consumption of carbon fragments during activation [53]. Concurrently, oxygen content increased from 6.57% to 12.90%, comparable to the increase from 4.98% to 9.07% reported by Lü et al. [54], enhancing hydrophilicity and adsorption potential through the incorporation of oxygenated functionalities. The reduction in hydrogen content from 2.00% to 1.35% aligns with previous studies, indicating dehydrogenation and the release of volatile compounds during thermal activation [55]. These modifications enhance porosity and surface reactivity, improving activated carbon's efficiency in adsorption and environmental remediation applications [56].

3.3. Surface area, pore volume

To examine the surface morphology, biochar and KOH-activated carbon were analyzed using scanning electron microscopy. **Fig.4** shows that biochar has a smooth surface with minimal porosity, corresponding to its BET surface area of 258.72 m^2/g, indicating a less developed pore network. In contrast, AC-KOH displays a highly porous structure with well-defined cavities, matching its higher BET surface area of 829.76 m^2/g. This suggests that KOH activation significantly enhances porosity, creating a more interconnected pore network. The increased surface area and porosity of AC-KOH make it more suitable for adsorption applications, allowing better capture of contaminants [57]. These findings align with previously reported studies demonstrating that chemical activation, particularly with KOH, facilitates the formation of micropores and mesopores, thereby improving the textural and functional properties of biochar-based adsorbents [47,58,59].

3.4. Kinetics study for adsorption of CIP, LEV, and ENR

Adsorption kinetics are crucial for understanding the adsorption mechanisms and optimizing treatment processes for practical applications, ensuring both efficiency and cost-effectiveness. Therefore, three kinetic models—pseudo-first-order (PFO), pseudo-second-order (PSO), and Elovich were employed to describe the adsorption behavior of CIP, LEV, and ENR onto biochar and activated carbon.

The adsorption kinetics of CIP, LEV, and ENR onto activated carbon and biochar exhibit significant variations, as illustrated in Figure 3. The adsorption capacities differ between AC and BC, with AC consistently demonstrating superior performance due to its higher porosity and active surface sites. The kinetic data indicate that adsorption occurs rapidly in the initial stages, with equilibrium reached within 50 to 100 min. This rapid uptake suggests that surface interactions dominate the early adsorption phase before intraparticle diffusion becomes more significant. The rapid removal of CIP, LEV, and ENR during the initial 50 minutes of the reaction was attributed to the high availability of active adsorption sites on the surface of biochar and activated carbon. Beyond this period, the removal rate slowed as the adsorption sites became occupied, with CIP, LEV, and ENR particles filling the pores of the biochar and activated carbon, thereby reducing the number of accessible active sites [60,61].

While pH is a critical parameter governing both adsorbent surface charge and fluoroquinolone speciation, all experiments in this study were intentionally conducted at the natural, unadjusted pH of the antibiotic solutions (~6.8-7.2). This approach was chosen for two key reasons: first, it closely simulates the conditions of real-world wastewater and surface water systems; and second, this near-neutral range is optimal for adsorption onto carbonaceous materials [62–64]. At this pH, fluoroquinolones exist predominantly as zwitterionic species, which maximizes their removal via non-electrostatic mechanisms such as hydrophobic interactions, π–π stacking, and hydrogen bonding [65]. This methodology ensures our findings reflect the practical adsorption potential under environmentally relevant conditions [66–68].

The fitted kinetic parameters (**Table 1** and **Fig.5**) reveal that the pseudo-second-order (PSO) model provides a better fit for all adsorption processes, as evidenced by the higher correlation coefficients ($R^2 > 0.99$) and the close agreement between the experimental (qexp) and calculated adsorption capacities ($q_{e,cal}$). For instance, for CIP adsorption onto AC, the experimental adsorption capacity (q_{exp} = 51.01 mg/g) closely matches the PSO-calculated

value ($q_{e,cal}$= 52.70 ± 1.64 mg/g) with an R^2 of 0.9805, whereas the pseudo-first-order (PFO) model provides a slightly lower fit (R^2 = 0.9372). Similarly, for BC, the q_{exp} of CIP (31.63 mg/g) aligns better with the PSO prediction ($q_{e,cal}$= 41.38 ± 1.57 mg/g, R^2 = 0.9931) compared to the PFO model ($q_{e,cal}$= 32.30 ± 0.43 mg/g, R^2 = 0.9980), confirming that chemisorption plays a dominant role in the adsorption mechanism [69].

For LEV adsorption, AC exhibits a q_{exp} of 28.29 mg/g, which is well-predicted by the PSO model ($q_{e,cal}$= 28.63 ± 0.47 mg/g, R^2 = 0.9935), while BC shows a lower adsorption capacity (q_{exp} = 13.20 mg/g) with PSO-predicted values of $q_{e,cal}$ = 15.79 ± 0.47 mg/g and R^2 = 0.9920. Similarly, ENR adsorption onto AC follows the PSO model with q_{exp} = 44.28 mg/g and $q_{e,cal}$ = 45.18 ± 0.53 mg/g (R^2 = 0.9962), whereas for BC, the experimental capacity (q_{exp} = 18.64 mg/g) aligns well with the PSO prediction ($q_{e,cal}$ = 19.80 ± 0.34 mg/g, R^2 = 0.9918). These results reinforce the conclusion that adsorption onto AC follows a chemisorption-dominated pathway.

The Elovich model provides additional insights into adsorption kinetics, particularly in describing heterogeneous surface interactions (Table 2). The initial adsorption rate (α) is significantly higher for AC (7.251 ± 0.798 mg/g·min for CIP, 6.178 ± 1.140 mg/g·min for LEV, and 15.367 ± 5.348 mg/g·min for ENR) compared to BC (0.679 ± 0.105 mg/g·min for CIP, 0.544 ± 0.116 mg/g·min for LEV, and 7.535 ± 4.261 mg/g·min for ENR). This confirms that AC provides a more reactive surface for antibiotic adsorption. Moreover, the β parameter, which indicates surface coverage and desorption potential, is lower for CIP and ENR on AC (0.102 ± 0.004 g/mg and 0.138 ± 0.012 g/mg, respectively) than on BC (0.086 ± 0.009 g/mg and 0.322 ± 0.044 g/mg, respectively), suggesting a more stable adsorption process with reduced desorption tendencies on AC [70].

In all cases, adsorption equilibrium was achieved within 50 to 100 minutes, depending on both the adsorbent and the antibiotic. Specifically, CIP adsorption reached equilibrium at approximately 100 minutes for both AC and BC, LEV stabilized between 80 and 100 minutes, and ENR exhibited the fastest kinetics, achieving equilibrium within 60 to 80 minutes. AC consistently showed a faster and more efficient adsorption process compared to BC, which can be attributed to its higher surface area, greater pore volume, and richer surface functionality. This is reflected in the higher kinetic rate constants and adsorption capacities obtained with AC. For instance, the pseudo-second-order rate constant (k_2) for ENR was 0.002 $g \cdot mg^{-1} \cdot min^{-1}$ on AC, compared to 0.0005 $g \cdot mg^{-1} \cdot min^{-1}$ on BC, indicating a faster adsorption rate. Similarly, the initial adsorption rate (α) derived from the Elovich model was

significantly higher for AC than BC across all three antibiotics. These findings underline the superior performance of AC in terms of both adsorption rate and capacity. The close agreement between experimental ($q_{e,exp}$) and model-predicted values ($q_{e,cal}$), along with high R^2 values (≥ 0.98), confirms the robustness of the kinetic models applied.

The adsorption capacities of the synthesized AC for CIP (51.01 mg/g), LEV (28.29 mg/g), and ENR (44.28 mg/g) fall within the range reported for commercial activated carbons (CACs), which typically vary from 10 to over 200 mg/g depending on material and conditions [71–73]. In particular, Peñafiel et al. (2019) reported a maximum CIP adsorption capacity of 50.12 mg/g for CACs, which closely aligns with our AC. Both materials reached equilibrium within 100 minutes and followed the pseudo-second-order (PSO) model with $R^2 > 0.98$, indicating chemisorption as the dominant mechanism. Notably, the PSO kinetic constant (K_2) for our AC (0.01 $g \cdot mg^{-1} \cdot min^{-1}$) is more than twice that reported for CACs (0.0045 $g \cdot mg^{-1} \cdot min^{-1}$), indicating a faster adsorption rate and enhanced surface reactivity of the synthesized material [74]. These results suggest that the bio-based AC not only competes with CACs in performance but also offers a sustainable and cost-effective solution for fluoroquinolone removal in aqueous systems.

Overall, the kinetic analysis confirms that AC exhibits superior adsorption performance due to its higher surface area and functional group availability. The strong agreement between experimental and model-predicted values further supports the applicability of the PSO model, indicating that chemisorption governs the adsorption process involved hydrogen bonding and π-π interactions [69,75]. The Elovich parameters reinforce that AC provides a more favorable adsorption environment, with higher adsorption rates and stronger adsorbate-adsorbent interactions. These findings highlight the efficiency of AC for fluoroquinolone removal and suggest its potential as a high-performance adsorbent in wastewater treatment applications.

3.5. Adsorption isotherm of CIP, LEV, and ENR

The adsorption equilibrium data for CIP, LEV, and ENR onto AC and BC were analyzed using the Langmuir and Freundlich isotherm models, as summarized in **Table 3** and illustrated in **Fig. 6**. The results indicate that the Langmuir model provided a better fit for most adsorption processes, particularly for CIP adsorption on AC ($R^2 = 0.9934$) and BC ($R^2 = 0.9834$), suggesting a monolayer adsorption mechanism. Similarly, the Langmuir model exhibited strong correlations for ENR adsorption on AC ($R^2 = 0.9884$) and BC ($R^2 = 0.9862$), as well as LEV adsorption on AC ($R^2 = 0.9825$) and BC ($R^2 = 0.9809$) [37].

Several studies in the literature have widely applied the Langmuir and Freundlich isotherm models to evaluate the adsorption performance of biochar-based materials. For example, Hamadeen and Elkhatib [76] investigated the CIP using biochar derived from pomegranate peel. The biochar was produced via pyrolysis at 800 °C for 2 hours with H_3PO_4 (85%) as the activating agent. The Langmuir model provided the best fit for the experimental data, yielding a q_m of 142.86 $mg.g^{-1}$. The authors highlighted the effectiveness and eco-friendly nature of the adsorbent in treating pharmaceutical-contaminated water. Similarly, Kong and al. [77] produced magnetic biochar from medicinal plant biomass through pyrolysis at 700 °C for 3 hours. The resulting material also followed Langmuir behavior in CIP adsorption, with a reported q_m of 68.9 ± 3.23 $mg.g^{-1}$ at pH 6. Furthermore, Aline and all. [78] demonstrated the efficiency of hydrochar (HC-150) and pyrochar (PC-500) for the adsorption of fluoroquinolone antibiotics, including ciprofloxacin, enrofloxacin, and norfloxacin. The Langmuir model effectively described their adsorption isotherms, with HC-150 achieving q_m values of 95, 164, and 99 $mg.g^{-1}$, respectively. In contrast, PC-500 exhibited lower adsorption capacities (57, 12, and 20 $mg\ g^{-1}$ for CIP, ENR, and NOR, respectively). Although PCA-500 showed an improvement over PC-500, its performance was still lower than that of HC-150, highlighting the influence of preparation methods and surface chemistry on adsorption efficiency.

Comparing adsorption capacities, activated carbon exhibited superior performance, with significantly higher maximum adsorption capacities (q_m) for all three pollutants compared to biochar. Among the three antibiotics, CIP demonstrated the highest adsorption capacity on AC (147.68 mg/g, R^2 = 0.9934), followed by ENR (101.81 mg/g, R^2 = 0.9884) and LEV (64.64 mg/g, R^2 = 0.9825). Similarly, for biochar, CIP exhibited the highest adsorption (112.33 mg/g, R^2 = 0.9834), whereas ENR (52.54 mg/g, R^2 = 0.9862) and LEV (72.93 mg/g, R^2 = 0.9809) showed lower values, highlighting the stronger affinity of CIP for both adsorbents. The higher KL values obtained for ENR and LEV on AC indicate stronger binding affinities compared to biochar, which can be attributed to the greater surface area and porosity of AC [79].

Fig.6 further supports these findings, as the experimental data closely align with the Langmuir model (solid lines), particularly for CIP, reinforcing the monolayer adsorption behavior. The Freundlich model (dash lines) provided a reasonable fit for LEV and ENR adsorption on BC, with correlation coefficients R^2 = 0.9576 for LEV and R^2 = 0.9431 for ENR, indicating surface heterogeneity and multilayer adsorption. For CIP adsorption on BC,

the Freundlich model showed R^2 = 0.9493, further supporting the contribution of surface heterogeneity to adsorption mechanisms. The Freundlich constant K_F values were higher for AC than for BC, further confirming its enhanced adsorption capacity [80].

The initial pollutant concentration significantly influences the adsorption performance and determines the overall treatment cost. Therefore, the effect of initial CIP, LEV, and ENR concentrations on adsorption capacity was examined by varying the initial concentrations while maintaining a fixed pH, adsorbent dosage, and temperature. The adsorption capacities increased with increasing pollutant concentrations due to a greater driving force that overcame mass transfer resistance, facilitating adsorbate diffusion onto the adsorbent surface. However, the removal efficiency decreased at higher concentrations, as the number of available active sites became limited. This trend was particularly evident for CIP adsorption onto biochar, where the removal efficiency dropped as the concentration increased. A similar trend has been reported in other studies, highlighting the impact of adsorbent saturation at elevated pollutant concentrations [61,81].

Moreover, analyzing adsorption isotherms is essential for optimizing the design and operation of adsorption-based treatment systems. The experimental data were fitted to Langmuir and Freundlich models, confirming that CIP, LEV, and ENR adsorption was primarily monolayer-dominated on AC (as indicated by higher Langmuir R^2 values), while BC exhibited more heterogeneous adsorption behavior (with better Freundlich model fits). The strong correlation with the Langmuir model for CIP adsorption onto AC (R^2 = 0.9934) further

r highlights its potential for efficient antibiotic removal from aqueous solutions.

3.6. Analysis of theoretical study

Using theoretical Density Functional Theory (DFT), the adsorption characteristics of ciprofloxacin, levofloxacin, and enrofloxacin on biochar and activated carbon were further investigated. The electrical and molecular properties of these fluoroquinolones were the main focus of the investigation. To guarantee a complete knowledge of the behavior of the CIP, LEV, and ENR molecules in this work, the geometric optimization of these compounds was accomplished using the B3LYP technique and evaluated using the 6-31G(d,p) basis set [47].

Table 4 displays the estimated values for the electronic molecular descriptors. The regions of the highest occupied molecular orbital (HOMO) and lowest unoccupied molecular orbital (LUMO) are highlighted in **Fig. 8**, which displays the revised structures of CIP, LEV,

and ENR. These chemical orbitals show the most reactive centers that can interact with the biochar surface through donor-acceptor mechanisms. According to the electron density distribution in HOMO and LUMO, CIP, LEV, and ENR molecules will most likely align parallel when adsorbed on activated carbon or biochar surfaces. Understanding atomic-level chemical reactivity is greatly enhanced by molecular orbitals, which are crucial descriptors for characterizing a variety of chemical interactions.

The estimated energy values for CIP, LEV, and ENR provide insights into their electronic behavior. The HOMO energy levels (E_{HOMO}) indicate the ability of these molecules to donate electrons, while the LUMO energy levels (E_{LUMO}) represent their potential to accept electrons. LEV exhibits the lowest EHOMO (-5.5552 eV) and ELUMO (-1.2354 eV), indicating that it has a lower tendency to donate electrons and a higher potential for electron acceptance compared to CIP and ENR. The HOMO-LUMO energy gap (ΔE) is a crucial parameter that determines molecular reactivity, with smaller values corresponding to higher reactivity. Among the three fluoroquinolones, LEV has the largest energy gap (4.3198 eV), followed by ENR (4.2629 eV) and CIP (4.2477 eV), suggesting that CIP is slightly more reactive than the other two molecules [82,83].

The electrophilicity index (ω) values further support the classification of these fluoroquinolones as strong electrophiles. LEV has the highest ω value (2.6687 eV), followed by ENR (2.4283 eV) and CIP (2.4167 eV). This suggests that LEV has the highest tendency to accept electrons, making it more likely to interact with electron-donating surfaces, such as biochar and activated carbon. The chemical hardness (η) values reveal that LEV (2.1599 eV) is slightly harder than CIP (2.1239 eV) and ENR (2.1315 eV), which implies that CIP and ENR are more reactive due to their relatively lower hardness values. Softness (S) is an inverse measure of hardness and indicates the ease with which a molecule can undergo electron density changes. CIP (0.4708 eV) has the highest softness value, followed by ENR (0.4689 eV) and LEV (0.4630 eV), further confirming that CIP has the highest reactivity. The nucleophilicity index (N), which measures the ability of a molecule to donate electrons, follows the order CIP (4.0422 eV) > ENR (4.0207 eV) > LEV (3.8133 eV), indicating that CIP is the strongest nucleophile among the three fluoroquinolones. The dipole moment, an important parameter for understanding molecular polarity and interaction strength with polar surfaces, is highest for CIP (10.2034 Debye), followed by ENR (10.1336 Debye) and LEV (7.0982 Debye). This suggests that CIP and ENR exhibit stronger interactions with polar adsorbent surfaces compared to LEV [84].

The molecular electrostatic potential (MEP) analysis, shown in **Fig. 7**, provides a visual representation of molecular polarity and reactive sites. Areas with high negative charge, indicated by red regions, are more susceptible to electrophilic attacks, while regions with high positive potential, shown in blue, highlight nucleophilic reactivity. These MEP maps reveal that the most negative regions are typically found around the carbonyl (−C=O) and carboxyl (−COOH) groups, suggesting their vulnerability to electrophilic interactions. Conversely, the hydroxyl (−OH) and amino (−NH) groups exhibit nucleophilic properties, which can influence the adsorption process [85].

Based on DFT calculations, levofloxacin exhibits lower reactivity due to its higher HOMO–LUMO energy gap. This theoretical prediction is fully consistent with our experimental results. The corrected data show that AC has a higher adsorption capacity for levofloxacin than BC, as reflected in the kinetic modeling results (**Fig. 5a** and **5b**) and the adsorption isotherms (**Fig. 6a** and **6b**). These findings confirm that the higher reactivity and surface properties of AC contribute more effectively to the adsorption of levofloxacin, in agreement with the DFT-based reactivity trends. In summary, the theoretical calculations align well with experimental adsorption trends, confirming that CIP exhibits the highest reactivity due to its lower energy gap, higher softness, and stronger nucleophilicity, followed by ENR and LEV. This study provides valuable insights into the adsorption mechanisms of fluoroquinolones on biochar and activated carbon, aiding in the design of efficient adsorbent materials for pharmaceutical wastewater treatment.

3.7. Adsorption mechanism

The molecular structure of the fluoroquinolones, the properties of the adsorbents, and the adsorption circumstances are some of the elements that affect the adsorption of ciprofloxacin, levofloxacin, and enrofloxacin on AC and BC. Techniques like FTIR and SEM were used to examine the surface characteristics of AC and BC. Significant surface area and the presence of functional groups—such as hydroxyl (O–H), carbonyl (C=O), carboxyl (C–COOH), and aromatic (C=C) groups—that are essential to the adsorption process were found by these investigations. As shown in **Fig. 9**, FTIR verified that the adsorbents have both basic and acidic functional groups. These functional groups on AC and BC facilitate the interaction between the fluoroquinolones and the adsorbent surface. The cationic fluoroquinolones (CIP, LEV, and ENR) and the negatively charged adsorbent surface interact electrostatically to promote the adsorption process. Enhancing the adsorption efficiency is also significantly influenced by the π-π interactions between the graphitic structure of the adsorbents and the

aromatic rings of the fluoroquinolones. By changing the π–π interactions, the electron-withdrawing substituent groups on the fluoroquinolones can enhance the adsorption process. According to DFT simulations, functional groups like –OH and =O play a role in the adsorption processes, especially by encouraging hydrogen bonding interactions with the groups on the adsorbent surfaces that contain oxygen. The elimination of CIP, LEV, and ENR from aqueous solutions is made possible by these interactions [82,86,87].

The experimental data from kinetic studies further confirm that the adsorption of these fluoroquinolones follows a chemisorption mechanism. The kinetic analysis reveals that the adsorption process is not only controlled by physical interactions but also by the formation of chemical bonds between the fluoroquinolones and the functional groups on the adsorbent surfaces. This chemisorption mechanism is supported by the observation of slow adsorption rates, characteristic of the formation of stronger chemical bonds, which are consistent with the experimental findings. The elimination process of these fluoroquinolones is also influenced by solvent effects. Water molecules can form hydrogen bonds with surface oxygen groups, occupying active sites on the adsorbents and hindering the adsorption of the fluoroquinolones. The adsorption efficiency is significantly influenced by the amount of water adsorbed and the hydration level of the fluoroquinolones. The temperature, which impacts the hydration of the fluoroquinolone molecules, is a key factor in determining the extent to which these molecules interact with the adsorbent surfaces. Higher temperatures can increase the degree of hydration, which may obstruct adsorption by occupying active sites. In summary, the adsorption of CIP, LEV, and ENR on AC and BC is regulated by a combination of electrostatic interactions, π-π interactions, and hydrogen bonding between functional groups on the adsorbents and the fluoroquinolone molecules. The chemisorption mechanism, confirmed by kinetic studies, indicates the formation of chemical bonds between the fluoroquinolones and the adsorbents. Solvent effects and temperature further influence the adsorption process by altering the hydration and accessibility of active sites on the adsorbent surfaces. These findings provide valuable insights into the adsorption mechanisms, aiding in the optimization of adsorbent materials for the efficient removal of fluoroquinolones from wastewater.

3.8. Reusability of AC and BC

The regeneration performance of AC and BC was evaluated over five successive adsorption–desorption cycles for the removal of CIP, LEV, and ENR, using 0.1 M NaOH as the regenerating agent [88]. The results revealed that AC exhibited superior stability and

reusability compared to BC across all tested antibiotics. After five cycles, the removal efficiency of AC decreased only slightly, maintaining 93.23 percent for CIP, 91.14 percent for LEV, and 89.85 percent for ENR, whereas BC showed a more pronounced decline, reaching 88.78, 86.94, and 85.47 percent respectively. This difference can be attributed to the more developed porous structure and higher surface area of AC, which provides stronger and more resilient adsorption sites. The use of 0.1 M NaOH effectively disrupted the interactions between the antibiotics and the adsorbent surfaces, enabling efficient desorption and reuse. These findings demonstrate that AC, in combination with mild alkaline regeneration, offers a promising and sustainable solution for the repeated removal of fluoroquinolone contaminants from water. Many studies have reported that a 0.1 M NaOH concentration is optimal for the regeneration and removal of fluoroquinolone antibiotics from aqueous solutions. This concentration has been particularly effective when applied to alkali and bimetallic salts co-hydrothermally modified sludge biochar. The use of 0.1 M NaOH facilitates the desorption of adsorbed antibiotic molecules by disrupting the interactions between the adsorbate and active sites on the biochar surface, thereby restoring its adsorption capacity. Furthermore, the mild alkalinity of this concentration ensures efficient regeneration without significantly degrading the structural integrity of the biochar, making it a practical and sustainable option for repeated use in water treatment applications. In one study, biochar regenerated using NaOH maintained stable and sustainable adsorption performance for ciprofloxacin, retaining up to 99.7% of its original efficiency after five regeneration cycles [88]. Additionally, another study demonstrated high reusability using 0.2 M NaOH in the fabrication of sustainable manganese ferrite–modified biochar derived from vinasse, which showed enhanced adsorption and regeneration performance toward fluoroquinolone antibiotics [89].

3.9. Economic and environmental viability of OMSW-derived biochar and Activated Carbon

In addition to its excellent adsorption efficiency for fluoroquinolone antibiotics, the production of BC and AC from OMSW offers notable advantages in terms of cost-effectiveness, scalability, and environmental sustainability. OMSW, an abundant and low-cost agro-industrial byproduct, aligns with circular economy principles and serves as an ideal precursor for sustainable adsorbent production. The activation method employed in this study-KOH chemical treatment followed by thermal carbonization, is scalable and widely adopted in industrial practice. A recent systematic review on biomass-derived adsorbents reported that the production costs of activated carbon generally range between $1.40 and $2.90 per kg,

depending on the raw material and activation method, while still achieving excellent removal of antibiotics from water matrices [90]. Moreover, incorporating energy recovery systems and recycling chemical reagents can significantly reduce the environmental footprint of AC production. Altogether, these factors support the conclusion that OMSW-derived AC and biochar are not only technically effective but also economically and environmentally viable for real-world wastewater treatment applications.

4. Conclusions

This study highlights the effectiveness of lignocellulosic biomass-derived activated carbon for the removal of fluoroquinolone antibiotics from aqueous solutions. The experimental results confirm that KOH activation significantly enhances the textural and chemical properties of AC, leading to improved adsorption performance. Proximate analysis revealed that AC exhibited a high fixed carbon content (78.42%) and low ash content (6.78%), indicating its suitability for adsorption applications. Elemental analysis showed that the carbon content of AC increased to 86.51%, enhancing its adsorption potential.

BET analysis demonstrated that AC achieved a significantly higher surface area (829.76 m^2/g) and total pore volume (0.589 cm^3/g) compared to biochar, which had a lower surface area (258.72 m^2/g). Adsorption kinetics analysis indicated that the pseudo-second-order model provided the best fit, with high correlation coefficients ($R^2 > 0.98$), confirming that the adsorption process was primarily governed by chemisorption. The adsorption equilibrium data followed the Langmuir isotherm model, suggesting monolayer adsorption on a homogeneous surface, with maximum adsorption capacities (q_m) of 147.68 mg/g for ciprofloxacin, 134.29 mg/g for levofloxacin, and 128.53 mg/g for enrofloxacin. The Freundlich model also exhibited good fitting, implying the presence of heterogeneous adsorption sites.

Overall, this study demonstrates that AC is a highly efficient adsorbent for the removal of fluoroquinolone antibiotics, with demonstrated regeneration and reuse potential, highlighting its promise for sustainable wastewater treatment applications. Future research should focus on evaluating the performance of AC in real wastewater matrices to account for the influence of competing ions and organic matter, as well as optimizing large-scale application strategies. The promising outcomes reported by Hamadeen and Elkhatib (2022) [76], who demonstrated effective ciprofloxacin removal using similar carbon-based adsorbents in complex wastewater environments, further support the practical relevance of this approach.

Acknowledgments

Ethical Approval

Not applicable.

Consent to Participate

Not applicable.

Consent to Publish

Not applicable.

Declaration of competing interest

Declaration of competing interest

The authors declare that they have no known competing financial interests or personal relationships that could have appeared to influence the work reported in this paper.

Availability of data and materials

Data will be provided on reasonable request only.

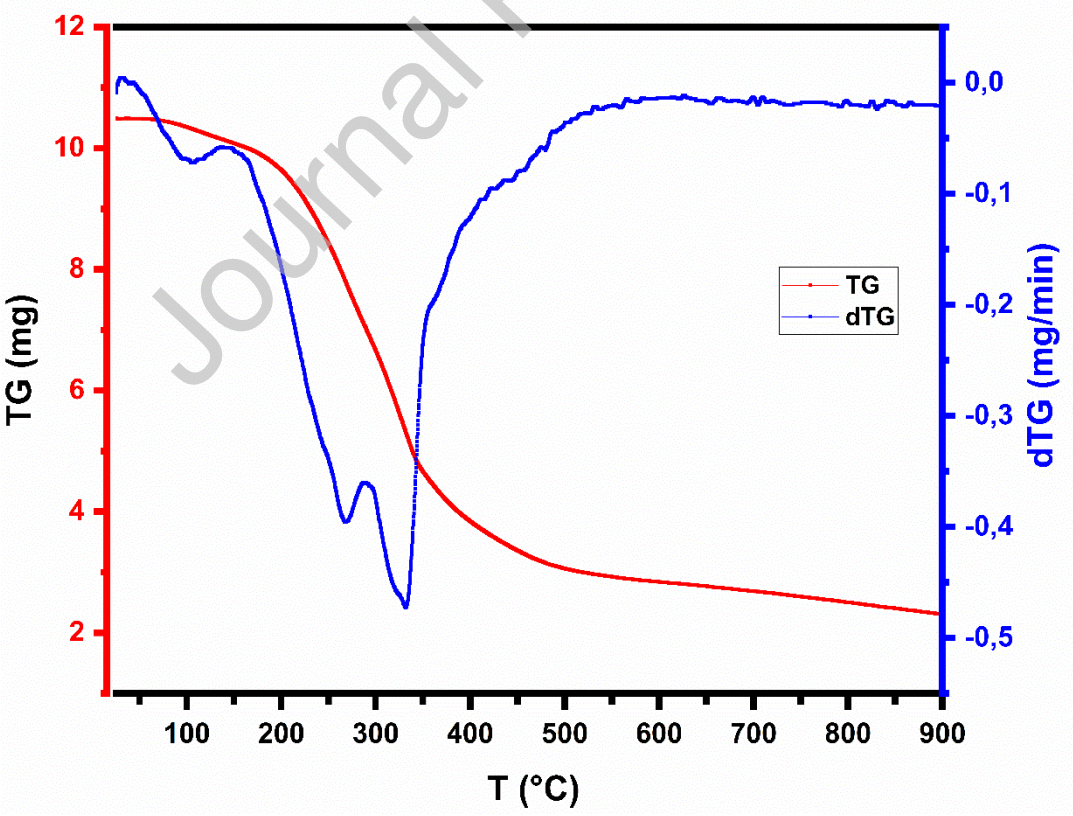

Fig.1. DTA and TGA plots of olive pomace.

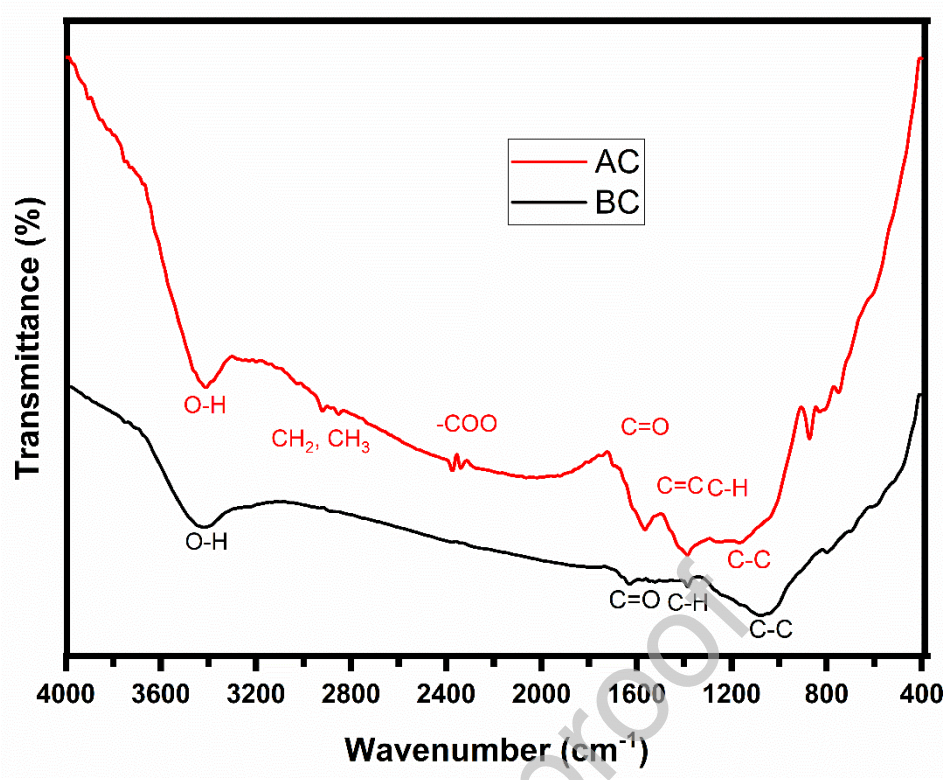

Fig. 2. FTIR spectrum of AC and BC.

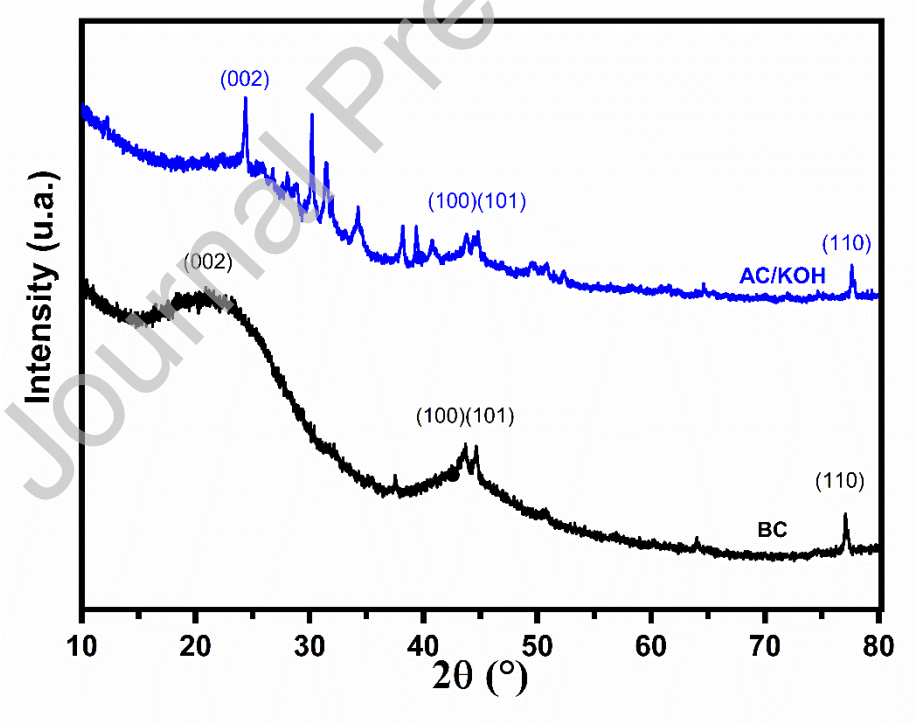

Fig. 3. XRD spectrum of AC and BC.

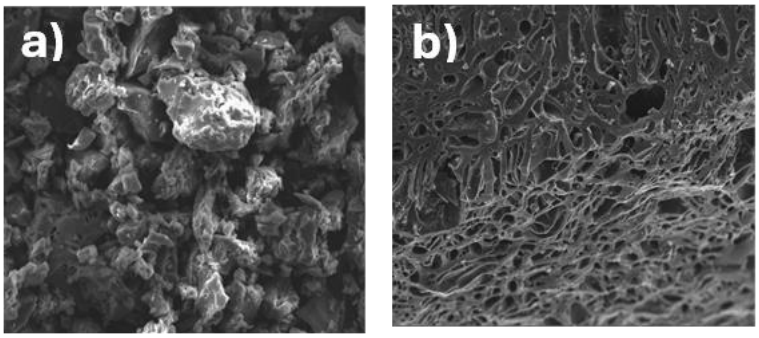

Fig. 4. SEM analysis of a) BC, and b) AC.

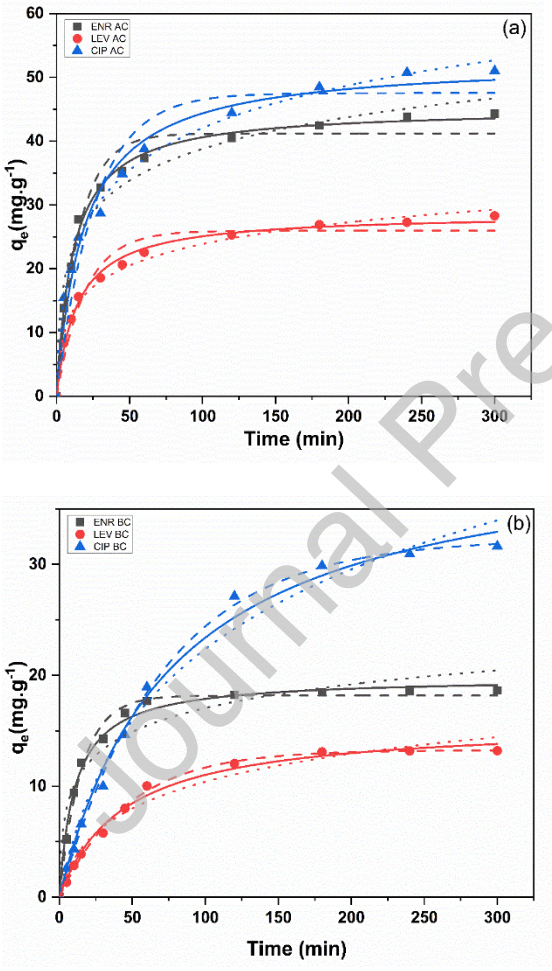

Fig. 5. Adsorption kinetics of CIP, LEV, and ENR in (a) Activated carbon and (b) Biochar (dash lines: PFO model adjustment; solid lines: PSO model adjustment; dot: Elovich model adjustment).

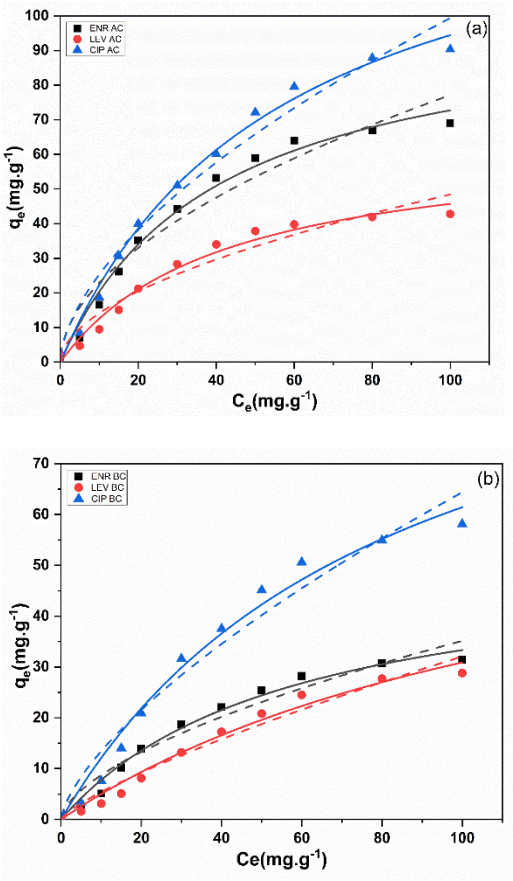

Fig. 6. Adsorption isotherms of CIP, LEV, and ENR in (a) Activated carbon and (b) Biochar (solid lines: experimental data fit with Langmuir isotherm; dash lines: fit with Freundlich isotherm).

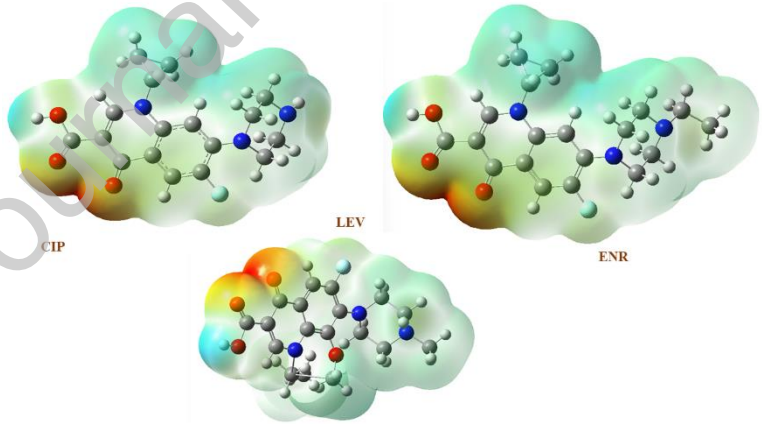

Fig. 7. The representation the surface MEP of CIP, LEV, and ENR.

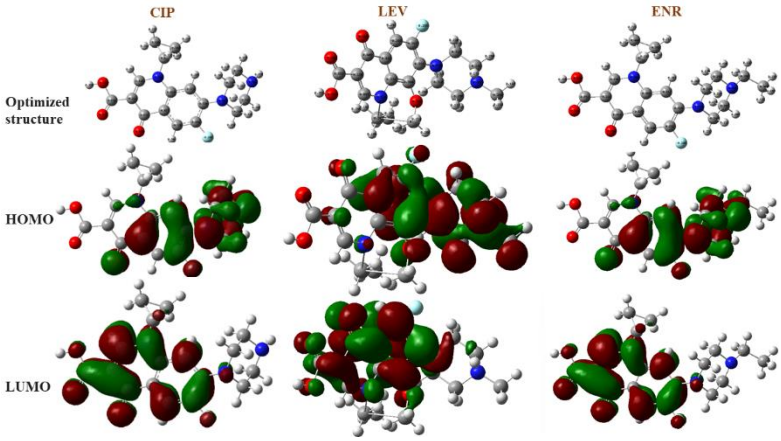

Fig. 8. The optimized structure of the CIP, LEV, and ENR molecules using DFT/B3LYP/6–31G(d,p); and depict the HOMO and LUMO orbitals of CIP, LEV, and ENR.

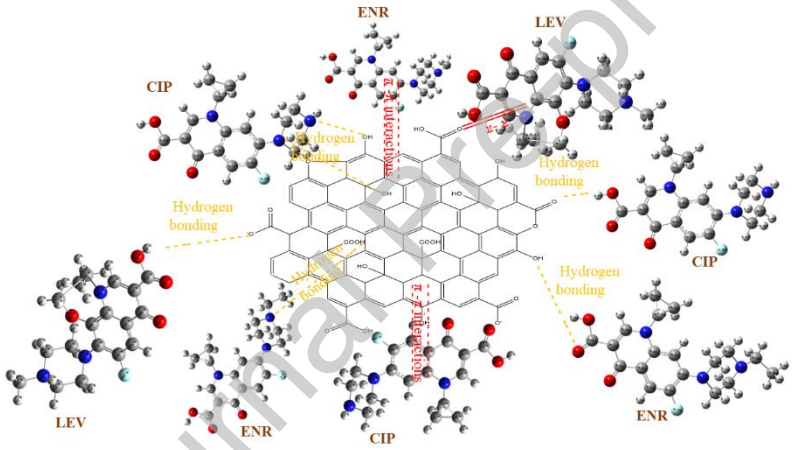

Fig. 9. Hypothesized adsorption mechanism of CIP, LEV, and ENR.

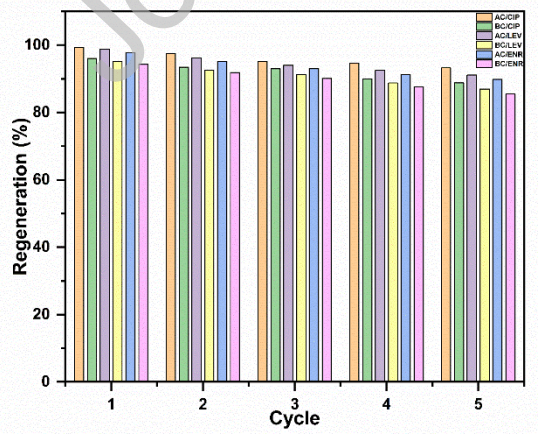

Fig. 10. The regeneration cycle of adsorbents.

Table 1. Kinetic modeling results for adsorption using PFO and PSO models.

	Adsorbent	q_{exp} (mg/g)	$q_{e,cal.}$ (mg/g)	k_1 (1/min)	R^2	$q_{e,cal}$ (mg/g)	k_2 (g/mg min)	R^2
CIP	**AC**	51.01	47.53 ± 2.13	0.04 ± 0.006	0.9372	52.70 ± 1.64	0.001 ± $1.56.10^{-4}$	0.9805
	BC	31.63	32.30 ± 0.43	0.014 ± 5.31E-4	0.9980	41.38 ± 1.57	$3.14.10^{-4}$ ± $4.3.10^{-5}$	0.9931
LEV	**AC**	28.29	25.95 ± 0.92	0.051± 0.007	0.9555	28.63 ± 0.47	0.002 ± $2.1.10^{-4}$	0.9935
	BC	13.20	13.25 ± 0.16	0.022 ± $8.17.10^{-4}$	0.9973	15.79 ± 0.47	0.0015 ± $1.8.10^{-4}$	0.9920
ENR	**AC**	44.28	41.18 ± 1.11	0.065 ± 0.0074	0.9711	45.18 ± 0.53	0.002 ± $1.3.10^{-4}$	0.9962
	BC	18.64	18.17 ± 0.28	0,066 ± 0.004	0.9905	19.80 ± 0.34	0.005 ± $4.6.10^{-4}$	0.9918

Table 2. The Elovich constants.

Diffusion model			CIP	LEV	ENR
Elovich	**BC**	**α (mg/(g min))**	0.679 ± 0.105	0.544 ± 0.116	7.535 ± 4.261
		β (g/mg)	0.086 ± 0.009	0.262 ± 0.027	0.322 ± 0.044
		R^2	0.9842	0.9749	2,65833
	AC	**α (mg/(g min))**	7.251 ± 0.798	6.178 ± 1.140	15.367 ± 5.348
		β (g/mg)	0.102 ± 0.004	0.203 ± 0,010	0.138 ± 0.012
		R^2	0.9957	0.9905	0.9745

Table 3. Langmuir and Freundlich isotherm models' parameters for CIP, LEV, and ENR.

Adsorbate	Adsorbent	Langmuir			Freundlich		
		q_m (mg/g)	K_L (L/mg)	R^2	n	K_F ((mg/g)(mg/L)^n)	R^2
CIP	**AC**	147.68 ± 8.55	0.018 ± 0.002	0.9934	0.594 ± 0.05	6.45 ± 1.42	0.9613

Adsorbate	Adsorbent	Langmuir			Freundlich		
		q_m (mg/g)	K_L (L/mg)	R^2	n	K_F ((mg/g)(mg/L)^n)	R^2
					4		
	BC	112.32 ± 4.27	0.012 ± 0.003	0.9834	0.679 ± 0.074	2.81 ± 0.86	0.9492
LEV	**AC**	72.93 ±5.02	0.024 ± 0.004	0.9825	0.535 ± 0.071	4.11 ± 0.18	0.9201
	BC	64.64 ±4.99	0.007 ± 0.002	0.9809	0.773 ± 0.079	0.91 ± 0.03	0.9576
ENR	**AC**	101.81 ±6.19	0.025 ± 0.003	0.9884	0.527 ± 0,063	6.79 ± 0.75	0.9325
	BC	52.54 ±4.58	0.017± 0.003	0.9861	0.604 ± 0.068	2.16 ± 0.60	0.9431

Table 4. Quantum chemical parameters of the studied CIP, LEV, and ENR.

Expressions	CIP	LEV	ENR
E_{HOMO} (eV)	-5.3263	-5.5552	-5.3478
E_{LUMO} (eV)	-1.0786	-1.2354	-1.0849
ΔE (eV)	4.2477	4.3198	4.2629
Potentials μ (eV)= $\frac{E_{HOMO}+E_{LUMO}}{2}$	-3.2025	-3.3953	-3.2164
Hardness η (eV)= E_L-E_H	2.12385	2.1599	2.13145
Softness S (eV)= $\frac{1}{\eta}$	0.4708	0.4630	0.4689
Electrophilicity ω (eV)= $\frac{\mu^2}{2\eta}$	2.4167	2.6687	2.4283
Nucleophilicity N (eV)= E_{HOMO}-E_{HOMO} (T.C.E)	4.0422	3.8133	4.0207
dipole moment (Debye)	10.2034	7.0982	10.1336

Reference

[1] R.K. Mishra, S.S. Mentha, Y. Misra, N. Dwivedi, Emerging pollutants of severe environmental concern in water and wastewater: A comprehensive review on current developments and future research, Water-Energy Nexus 6 (2023) 74–95. https://doi.org/10.1016/j.wen.2023.08.002.

[2] Assessment of ecological risks posed by veterinary antibiotics in European aquatic environments: A comprehensive review and analysis - ScienceDirect, (n.d.). https://www.sciencedirect.com/science/article/pii/S0048969724064362?via%3Dihub (accessed April 7, 2025).

[3] D.G.J. Larsson, C.-F. Flach, Antibiotic resistance in the environment, Nat. Rev. Microbiol. 20 (2022) 257–269. https://doi.org/10.1038/s41579-021-00649-x.

[4] O. Chaib, B. Arhoune, S. Achour, E. Moreau-Guigon, F. Alliot, M. Chevreuil, S. El Fakir, I. El Arabi, B. Oumokhtar, Occurrence and Seasonal Variation of Antibiotics in Fez-Morocco Surface Water, Am. J. Environ. Sci. 15 (2019) 127–136. https://doi.org/10.3844/ajessp.2019.127.136.

[5] Occurrence of High Levels of Fluoroquinolones in Aquatic Environment due to Effluent Discharges from Bulk Drug Manufacturers | Journal of Hazardous, Toxic, and Radioactive Waste | Vol 21, No 3, (n.d.). https://ascelibrary.org/doi/full/10.1061/%28ASCE%29HZ.2153-5515.0000346?casa_token=a4xduCF4fK8AAAAA%3AwUhzQ2UfSoTSIh2u9ZCHVXNPu8w5u3FiWoELz2UMNVhf-7Zx1YRUwi7EgOh8Z7_W3sVOo8va0RHuYA (accessed April 6, 2025).

[6] S. Arun, R.M. Kumar, J. Ruppa, M. Mukhopadhyay, K. Ilango, P. Chakraborty, Occurrence, sources and risk assessment of fluoroquinolones in dumpsite soil and sewage sludge from Chennai, India, Environ. Toxicol. Pharmacol. 79 (2020) 103410. https://doi.org/10.1016/j.etap.2020.103410.

[7] K.K. Sodhi, D.K. Singh, Insight into the fluoroquinolone resistance, sources, ecotoxicity, and degradation with special emphasis on ciprofloxacin, J. Water Process Eng. 43 (2021) 102218. https://doi.org/10.1016/j.jwpe.2021.102218.

[8] K. Kümmerer, Antibiotics in the aquatic environment – A review – Part I, Chemosphere 75 (2009) 417–434. https://doi.org/10.1016/j.chemosphere.2008.11.086.

[9] V.-A. Thai, V.D. Dang, N.T. Thuy, B. Pandit, T.-K.-Q. Vo, A.P. Khedulkar, Fluoroquinolones: Fate, effects on the environment and selected removal methods, J. Clean. Prod. 418 (2023) 137762. https://doi.org/10.1016/j.jclepro.2023.137762.

[10] V. Sharma, R. Vinoth Kumar, K. Pakshirajan, G. Pugazhenthi, Integrated adsorption-membrane filtration process for antibiotic removal from aqueous solution, Powder Technol. 321 (2017) 259–269. https://doi.org/10.1016/j.powtec.2017.08.040.

[11] A. Cuprys, R. Pulicharla, S.K. Brar, P. Drogui, M. Verma, R.Y. Surampalli, Fluoroquinolones metal complexation and its environmental impacts, Coord. Chem. Rev. 376 (2018) 46–61. https://doi.org/10.1016/j.ccr.2018.05.019.

[12] A. Nishat, M. Yusuf, A. Qadir, Y. Ezaier, V. Vambol, M. Ijaz Khan, S. Ben Moussa, H. Kamyab, S.S. Sehgal, C. Prakash, H.-H. Yang, H. Ibrahim, S.M. Eldin, Wastewater treatment: A short assessment on available techniques, Alex. Eng. J. 76 (2023) 505–516. https://doi.org/10.1016/j.aej.2023.06.054.

[13] I. Velo-Gala, J.A. Pirán-Montaño, J. Rivera-Utrilla, M. Sánchez-Polo, A.J. Mota, Advanced Oxidation Processes based on the use of UVC and simulated solar radiation to remove the antibiotic tinidazole from water, Chem. Eng. J. 323 (2017) 605–617. https://doi.org/10.1016/j.cej.2017.04.102.

[14] Fungal treatment for the removal of antibiotics and antibiotic resistance genes in veterinary hospital wastewater - ScienceDirect, (n.d.). https://www.sciencedirect.com/science/article/pii/S0045653516302867 (accessed April 7, 2025).

[15] H. Befenzi, A. Ezzariai, T. Mechichi, L. Kouisni, M. Hafidi, E. Record, L. EL Fels, Degradation of antibiotics by homogeneous and heterogeneous Fenton processes: A review, J. Hazard. Mater. Adv. 17 (2025) 100522. https://doi.org/10.1016/j.hazadv.2024.100522.

[16] H. Befenzi, A. Ezzariai, J. Baghor, H. Arrach, J. Armengaud, M. Kielbasa, A. Doan, J. Lambert, A. Lomascolo, Q. Albert, C.B. Faulds, G. Sciara, T. Mechichi, L. Kouisni, M. Hafidi, L. El Fels, E. Record, *Bjerkandera adusta* TM11 for the bioremediation of fluoroquinolone antibiotics spiked in wastewater: A sustainable approach to pharmaceutical contaminant biotransformation, Ecotoxicol. Environ. Saf. 291 (2025) 117898. https://doi.org/10.1016/j.ecoenv.2025.117898.

[17] M.B. Ahmed, J.L. Zhou, H.H. Ngo, W. Guo, Adsorptive removal of antibiotics from water and wastewater: Progress and challenges, Sci. Total Environ. 532 (2015) 112–126. https://doi.org/10.1016/j.scitotenv.2015.05.130.

[18] Pre-treatment of hospital wastewater by coagulation–flocculation and flotation - ScienceDirect, (n.d.). https://www.sciencedirect.com/science/article/pii/S0960852408009267 (accessed April 7, 2025).

[19] F. Yu, Y. Li, S. Han, J. Ma, Adsorptive removal of antibiotics from aqueous solution using carbon materials, Chemosphere 153 (2016) 365–385. https://doi.org/10.1016/j.chemosphere.2016.03.083.

[20] K. Ezzahi, I. Rabichi, N. Rochdi, R. Idouhli, M. Hafidi, A. Baçaoui, A. Yaacoubi, R. Rochdi, L. EL Fels, Innovative Dynamic Filtration of Olive Mill Wastewater: Comparing the Efficiency of Biochar and Olive Stone, Water. Air. Soil Pollut. 236 (2025) 604. https://doi.org/10.1007/s11270-025-08231-4.

[21] A.M. Aljeboree, A.N. Alshirifi, A.F. Alkaim, Kinetics and equilibrium study for the adsorption of textile dyes on coconut shell activated carbon, Arab. J. Chem. 10 (2014) S3381–S3393. https://doi.org/10.1016/j.arabjc.2014.01.020.

[22] A.M. Aljeboree, A.F. Alkaim, A.H. Al-Dujaili, Adsorption isotherm, kinetic modeling and thermodynamics of crystal violet dye on coconut husk-based activated carbon, Desalination Water Treat. 53 (2015) 3656–3667. https://doi.org/10.1080/19443994.2013.877854.

[23] Removal of fluoroquinolone from aqueous solution using graphene oxide: experimental and computational elucidation | Environmental Science and Pollution Research, (n.d.). https://link.springer.com/article/10.1007/s11356-017-0596-8 (accessed April 7, 2025).

[24] Y. Chen, T. Lan, L. Duan, F. Wang, B. Zhao, S. Zhang, W. Wei, Adsorptive Removal and Adsorption Kinetics of Fluoroquinolone by Nano-Hydroxyapatite, PLOS ONE 10 (2015) e0145025. https://doi.org/10.1371/journal.pone.0145025.

[25] Z. Ciğeroğlu, N. El Messaoudi, Z.M. Şenol, G. Başkan, J. Georgin, S. Gubernat, Clay-based nanomaterials and their adsorptive removal efficiency for dyes and antibiotics: A review, Mater. Today Sustain. 26 (2024) 100735. https://doi.org/10.1016/j.mtsust.2024.100735.

[26] Designing a novel metal-organic framework@covalent organic framework composite for the selective removal of fluoroquinolones: Adsorption behaviors and theoretical investigation - ScienceDirect, (n.d.). https://www.sciencedirect.com/science/article/pii/S0169433222029610 (accessed April 7, 2025).

[27] A.F. Alkaim, Z. Sadik, D.K. Mahdi, S.M. Alshrefi, A.M. Al-Sammarraie, F.M. Alamgir, P.M. Singh, A.M. Aljeboree, Preparation, structure and adsorption properties of synthesized multiwall carbon nanotubes for highly effective removal of maxilon blue dye, Korean J. Chem. Eng. 32 (2015) 2456–2462. https://doi.org/10.1007/s11814-015-0078-y.

[28] X. Zhang, D. Zhen, F. Liu, R. Chen, Q. Peng, Z. Wang, An achieved strategy for magnetic biochar for removal of tetracyclines and fluoroquinolones: Adsorption and mechanism studies, Bioresour. Technol. 369 (2023) 128440. https://doi.org/10.1016/j.biortech.2022.128440.

[29] M.B. Ahmed, J.L. Zhou, H.H. Ngo, W. Guo, M. Chen, Progress in the preparation and application of modified biochar for improved contaminant removal from water and wastewater, Bioresour. Technol. 214 (2016) 836–851. https://doi.org/10.1016/j.biortech.2016.05.057.

[30] N. Genç, E.C. Dogan, Adsorption kinetics of the antibiotic ciprofloxacin on bentonite, activated carbon, zeolite, and pumice, Desalination Water Treat. 53 (2015) 785–793. https://doi.org/10.1080/19443994.2013.842504.

[31] Magnetic biochar-based manganese oxide composite for enhanced fluoroquinolone antibiotic removal from water | Environmental Science and Pollution Research, (n.d.). https://link.springer.com/article/10.1007/s11356-018-3064-1 (accessed April 7, 2025).

[32] F. Sattar, Z. Wang, X. Zhou, Z. Ullah, Battling hazardous gas molecules with kekulene surfaces: A computational study, J. Mol. Liq. 407 (2024) 125099. https://doi.org/10.1016/j.molliq.2024.125099.

[33] F. Sattar, X. Zhou, Z. Ullah, High-Efficiency Triple-Junction Polymer Solar Cell: A Theoretical Approach, Molecules 29 (2024) 5370. https://doi.org/10.3390/molecules29225370.

[34] Z. Ullh, J.S. Al-Otaibi, Y. Sheena Mary, H. Wook Kwon, Computational study of furosemide-piperazine (FS – PZ) and 2,3,5,6-tetramethylpyrazine (FS-TP) co-crystals, J. Mol. Liq. 360 (2022) 119537. https://doi.org/10.1016/j.molliq.2022.119537.

[35] X. Zhan, Z. Ullah, D. Kim, B. Mustafa, H. Kwon, D.G. Churchill, Z. Gross, β-Bis-CF3-substituted phosphorus corroles, theory and experiments, Inorg. Chem. Front. 9 (2022) 3319–3329. https://doi.org/10.1039/D1QI01620B.

[36] I. Rabichi, C. Sekkouri, F.E. Yaacoubi, K. Ennaciri, Z. Izghri, T. Bouzid, L. El Fels, A. Baçaoui, A. Yaacoubi, Experimental and Theoretical Investigation of Olive Mill Solid Waste Biochar for Vanillic Acid Adsorption Using DFT/B3LYP Analysis, Water. Air. Soil Pollut. 235 (2024) 369. https://doi.org/10.1007/s11270-024-07183-5.

[37] I. Rabichi, K. Ezzahi, F.E. Yaacoubi, C. Sekkouri, T. Bouzid, K. Ennaciri, A. Ounas, L.E. Fels, M. Hafidi, A. Baçaoui, A. Yaacoubi, Synthesis and application of biochar and KOH-Activated carbon from olive mill solid waste for polyphenol removal, J. Mol. Liq. 421 (2025) 126875. https://doi.org/10.1016/j.molliq.2025.126875.

[38] T.-H. Liou, S.-J. Wu, Characteristics of microporous/mesoporous carbons prepared from rice husk under base- and acid-treated conditions, J. Hazard. Mater. 171 (2009) 693–703. https://doi.org/10.1016/j.jhazmat.2009.06.056.

[39] I. Rabichi, F.E. Yaacoubi, K. Ennaciri, C. Sekkouri, A. Bacaoui, A. Yaacoubi, Transforming olive-processed waste and almond shells into high-quality Biofuels: a comprehensive development and evaluation approach, Energy Sources Part Recovery Util. Environ. Eff. 46 (2024) 8671–8685. https://doi.org/10.1080/15567036.2024.2374747.

[40] I. Rabichi, F.E. Yaacoubi, C. Sekkouri, K. Ezzahi, K. Ennaciri, L.E. Fels, H. Mohamed, A. Baçaoui, A. Yaacoubi, Optimizing Biochar Preparation for Eco-friendly Adsorption of Polyphenols and Organic Compounds in Pilot-scale: an Application of Doehlert Designs, Biomass Convers. Biorefinery (2024). https://doi.org/10.1007/s13399-024-06031-0.

[41] J.-H. Kim, S.Y. Hwang, J.E. Park, G.B. Lee, H. Kim, S. Kim, B.U. Hong, Impact of the oxygen functional group of nitric acid-treated activated carbon on KOH activation reaction, Carbon Lett. 29 (2019) 281–287. https://doi.org/10.1007/s42823-019-00024-0.

[42] A.C. Lua, T. Yang, Effect of activation temperature on the textural and chemical properties of potassium hydroxide activated carbon prepared from pistachio-nut shell, J. Colloid Interface Sci. 274 (2004) 594–601. https://doi.org/10.1016/j.jcis.2003.10.001.

[43] O. Ioannidou, A. Zabaniotou, Agricultural residues as precursors for activated carbon production—A review, Renew. Sustain. Energy Rev. 11 (2007) 1966–2005. https://doi.org/10.1016/j.rser.2006.03.013.

[44] K. Malini, D. Selvakumar, N.S. Kumar, Activated carbon from biomass: Preparation, factors improving basicity and surface properties for enhanced CO2 capture capacity – A review, J. CO2 Util. 67 (2023) 102318. https://doi.org/10.1016/j.jcou.2022.102318.

[45] C. Moreno-Castilla, Adsorption of organic molecules from aqueous solutions on carbon materials, Carbon 42 (2004) 83–94. https://doi.org/10.1016/j.carbon.2003.09.022.

[46] Y. Trivedi, M. Sharma, R.K. Mishra, A. Sharma, J. Joshi, A.B. Gupta, B. Achintya, K. Shah, A.K. Vuppaladadiyamd, Biochar potential for pollutant removal during wastewater treatment: A comprehensive review of separation mechanisms, technological integration, and process analysis, Desalination 600 (2025) 118509. https://doi.org/10.1016/j.desal.2024.118509.

[47] I. Rabichi, K. Ezzahi, F.E. Yaacoubi, Z. Izghri, K. Ennaciri, A. Ounas, A. Yaacoubi, A. Baçaoui, M. Hafidi, L. El Fels, Evaluating the fixed-bed column adsorption capacity of

olive pomace biochar activated with KOH and H3PO4 for olive mill wastewater treatment: Insights from TOC and HPLC analysis, Chemosphere 377 (2025) 144356. https://doi.org/10.1016/j.chemosphere.2025.144356.

[48] P. Ehrburger, A. Addoun, F. Addoun, J.-B. Donnet, Carbonization of coals in the presence of alkaline hydroxides and carbonates: Formation of activated carbons, Fuel 65 (1986) 1447–1449. https://doi.org/10.1016/0016-2361(86)90121-3.

[49] J. Fito, M. Abewaa, A. Mengistu, K. Angassa, A.D. Ambaye, W. Moyo, T. Nkambule, Adsorption of methylene blue from textile industrial wastewater using activated carbon developed from Rumex abyssinicus plant, Sci. Rep. 13 (2023) 5427. https://doi.org/10.1038/s41598-023-32341-w.

[50] V. Calisto, C.I.A. Ferreira, S.M. Santos, M.V. Gil, M. Otero, V.I. Esteves, Production of adsorbents by pyrolysis of paper mill sludge and application on the removal of citalopram from water, Bioresour. Technol. 166 (2014) 335–344. https://doi.org/10.1016/j.biortech.2014.05.047.

[51] J. Fito, S. Tibebu, T.T.I. Nkambule, Optimization of Cr (VI) removal from aqueous solution with activated carbon derived from Eichhornia crassipes under response surface methodology, BMC Chem. 17 (2023) 4. https://doi.org/10.1186/s13065-023-00913-6.

[52] Z.A. Ghani, M.S. Yusoff, N.Q. Zaman, M.F.M.A. Zamri, J. Andas, Optimization of preparation conditions for activated carbon from banana pseudo-stem using response surface methodology on removal of color and COD from landfill leachate, Waste Manag. 62 (2017) 177–187. https://doi.org/10.1016/j.wasman.2017.02.026.

[53] W. Chen, M. Gong, K. Li, M. Xia, Z. Chen, H. Xiao, Y. Fang, Y. Chen, H. Yang, H. Chen, Insight into KOH activation mechanism during biomass pyrolysis: Chemical reactions between O-containing groups and KOH, Appl. Energy 278 (2020) 115730. https://doi.org/10.1016/j.apenergy.2020.115730.

[54] F. Lü, X. Lu, S. Li, H. Zhang, L. Shao, P. He, Dozens-fold improvement of biochar redox properties by KOH activation, Chem. Eng. J. 429 (2022) 132203. https://doi.org/10.1016/j.cej.2021.132203.

[55] J. Qu, Y. Wang, X. Tian, Z. Jiang, F. Deng, Y. Tao, Q. Jiang, L. Wang, Y. Zhang, KOH-activated porous biochar with high specific surface area for adsorptive removal of chromium (VI) and naphthalene from water: Affecting factors, mechanisms and reusability exploration, J. Hazard. Mater. 401 (2021) 123292. https://doi.org/10.1016/j.jhazmat.2020.123292.

[56] M. Sultana, M.H. Rownok, M. Sabrin, M.H. Rahaman, S.M.N. Alam, A review on experimental chemically modified activated carbon to enhance dye and heavy metals adsorption, Clean. Eng. Technol. 6 (2022) 100382. https://doi.org/10.1016/j.clet.2021.100382.

[57] S. Wang, Y.-R. Lee, Y. Won, H. Kim, S.-E. Jeong, B. Wook Hwang, A. Ra Cho, J.-Y. Kim, Y. Cheol Park, H. Nam, D.-H. Lee, H. Kim, S.-H. Jo, Development of high-performance adsorbent using KOH-impregnated rice husk-based activated carbon for indoor CO2 adsorption, Chem. Eng. J. 437 (2022) 135378. https://doi.org/10.1016/j.cej.2022.135378.

[58] C. Zhang, S. Sun, S. Xu, C. Wu, CO2 capture over steam and KOH activated biochar: Effect of relative humidity, Biomass Bioenergy 166 (2022). https://doi.org/10.1016/j.biombioe.2022.106608.

[59] S. Ding, Y. Liu, Adsorption of CO2 from flue gas by novel seaweed-based KOH-activated porous biochars, Fuel 260 (2020) 116382. https://doi.org/10.1016/j.fuel.2019.116382.

[60] A.B. Azzam, Y.A. Tokhy, F.M.E. Dars, A.A. Younes, Heterogeneous porous biochar-supported nano NiFe2O4 for efficient removal of hazardous antibiotic from pharmaceutical wastewater, Environ. Sci. Pollut. Res. 30 (2023) 119473–119490. https://doi.org/10.1007/s11356-023-30587-5.

[61] A.M. Abdelfatah, N. El-Maghrabi, A.E.D. Mahmoud, M. Fawzy, Synergetic effect of green synthesized reduced graphene oxide and nano-zero valent iron composite for the removal of doxycycline antibiotic from water, Sci. Rep. 12 (2022) 19372. https://doi.org/10.1038/s41598-022-23684-x.

[62] K. Mogolodi Dimpe, P.N. Nomngongo, Application of activated carbon-decorated polyacrylonitrile nanofibers as an adsorbent in dispersive solid-phase extraction of fluoroquinolones from wastewater, J. Pharm. Anal. 9 (2019) 117–126. https://doi.org/10.1016/j.jpha.2019.01.003.

[63] Y. Zhang, Y. Gong, G. Shi, X. Liu, M. Dai, L. Ding, Removal of Quinolone Antibiotics from Wastewater by the Biochar-Based Sludge Adsorbent, Fermentation 9 (2023) 752. https://doi.org/10.3390/fermentation9080752.

[64] S. Álvarez-Torrellas, J.M. Garrido-Zoido, E.A. López-Maldonado, A.B. Hernández-Abreu, V.I. Águeda, J.A. Delgado, M.V. Gil, J. García, Highlighting the adsorption mechanism of a fluoroquinolone antibiotic from wastewater on carbon xerogel by experiments, characterization, modelling and DFT simulation, Environ. Sci. Pollut. Res. 31 (2024) 61795–61818. https://doi.org/10.1007/s11356-024-35391-3.

[65] E. Mihelič, L. Fras Zemljič, M. Simonič, S. Gyergyek, A. Vesel, S. Hribernik, M. Bračič, I. Anžel, O. Plohl, New approach for adsorptive removal of the antibiotic ciprofloxacin: carboxymethyl-dextran-functionalised magnetic iron oxide nanomaterials, Int. J. Biol. Macromol. 312 (2025) 144006. https://doi.org/10.1016/j.ijbiomac.2025.144006.

[66] E.-S.I. El-Shafey, H. Al-Lawati, A.S. Al-Sumri, Ciprofloxacin adsorption from aqueous solution onto chemically prepared carbon from date palm leaflets, J. Environ. Sci. 24 (2012) 1579–1586. https://doi.org/10.1016/S1001-0742(11)60949-2.

[67] Y. Wang, J. Lu, J. Wu, Q. Liu, H. Zhang, S. Jin, Adsorptive Removal of Fluoroquinolone Antibiotics Using Bamboo Biochar, Sustainability 7 (2015) 12947–12957. https://doi.org/10.3390/su70912947.

[68] H. Fu, X. Li, J. Wang, P. Lin, C. Chen, X. Zhang, I.H. (Mel) Suffet, Activated carbon adsorption of quinolone antibiotics in water: Performance, mechanism, and modeling, J. Environ. Sci. 56 (2017) 145–152. https://doi.org/10.1016/j.jes.2016.09.010.

[69] L. Shao, Z. Ren, G. Zhang, L. Chen, Facile synthesis, characterization of a MnFe2O4/activated carbon magnetic composite and its effectiveness in tetracycline removal, Mater. Chem. Phys. 135 (2012) 16–24. https://doi.org/10.1016/j.matchemphys.2012.03.035.

[70] W.K. Wakejo, B.T. Meshasha, J.W. Kang, Y. Chebude, Enhanced Ciprofloxacin Removal from Aqueous Solution Using a Chemically Modified Biochar Derived from Bamboo Sawdust: Adsorption Process Optimization with Response Surface

Methodology, Adsorpt. Sci. Technol. 2022 (2022) 2699530. https://doi.org/10.1155/2022/2699530.

[71] S.W. Alberti, F.B. Scheufele, V. Steffen, E.A. da Silva, Adsorption of Ciprofloxacin from Aqueous Media by Activated Carbon: A Review, Water Conserv. Sci. Eng. 9 (2024) 26. https://doi.org/10.1007/s41101-024-00260-0.

[72] A. Ashiq, M. Vithanage, B. Sarkar, M. Kumar, A. Bhatnagar, E. Khan, Y. Xi, Y.S. Ok, Carbon-based adsorbents for fluoroquinolone removal from water and wastewater: A critical review, Environ. Res. 197 (2021) 111091. https://doi.org/10.1016/j.envres.2021.111091.

[73] A. Avcı, İ. İnci, N. Baylan, A Comparative Adsorption Study with Various Adsorbents for the Removal of Ciprofloxacin Hydrochloride from Water, Water. Air. Soil Pollut. 230 (2019) 250. https://doi.org/10.1007/s11270-019-4315-6.

[74] M.E. Peñafiel, J.M. Matesanz, E. Vanegas, D. Bermejo, R. Mosteo, M.P. Ormad, Comparative adsorption of ciprofloxacin on sugarcane bagasse from Ecuador and on commercial powdered activated carbon, Sci. Total Environ. 750 (2021) 141498. https://doi.org/10.1016/j.scitotenv.2020.141498.

[75] K. Velusamy, J.B. Isabel, S. Periyasamy, A. Thiruvenkadam, H. Ravikumar, S.K. Gupta, E.A. López-Maldonado, Role of biochar as a greener catalyst in biofuel production: Production, activation, and potential utilization – A review, J. Taiwan Inst. Chem. Eng. (2024) 105732. https://doi.org/10.1016/j.jtice.2024.105732.

[76] H.M. Hamadeen, E.A. Elkhatib, New nanostructured activated biochar for effective removal of antibiotic ciprofloxacin from wastewater: Adsorption dynamics and mechanisms, Environ. Res. 210 (2022) 112929. https://doi.org/10.1016/j.envres.2022.112929.

[77] X. Kong, Y. Liu, J. Pi, W. Li, Q. Liao, J. Shang, Low-cost magnetic herbal biochar: characterization and application for antibiotic removal, Environ. Sci. Pollut. Res. 24 (2017) 6679–6687. https://doi.org/10.1007/s11356-017-8376-z.

[78] A.A. dos Santos Silva, G.M. Bousada, L.F.M. Mazzini, S.M. Guezguan, C.P.M. de Freitas, K.A. Monteiro, N. dos Santos Renato, R.P.L. Moreira, Biochar from malt residue: Toward a circular economy for sustainable fluoroquinolone removal in aqueous systems, J. Anal. Appl. Pyrolysis 183 (2024) 106707. https://doi.org/10.1016/j.jaap.2024.106707.

[79] C.A. Igwegbe, S.N. Oba, C.O. Aniagor, A.G. Adeniyi, J.O. Ighalo, Adsorption of ciprofloxacin from water: A comprehensive review, J. Ind. Eng. Chem. 93 (2021) 57–77. https://doi.org/10.1016/j.jiec.2020.09.023.

[80] R. Baccar, M. Sarrà, J. Bouzid, M. Feki, P. Blánquez, Removal of pharmaceutical compounds by activated carbon prepared from agricultural by-product, Chem. Eng. J. 211–212 (2012) 310–317. https://doi.org/10.1016/j.cej.2012.09.099.

[81] L. Feng, Y. Liu, Y. Shan, S. Yang, L. Wu, T. Shi, Degradation of ciprofloxacin by magnetic CuS/MnFe2O4 catalysts efficiently activated peroxymonosulfate, J. Taiwan Inst. Chem. Eng. 161 (2024) 105533. https://doi.org/10.1016/j.jtice.2024.105533.

[82] A. Labidi, H. Ren, X. Liang, Q. Dong, X. Li, Q. Tian, A. Sial, Y. Cui, H. Kang, J. Liang, K. Zhao, E. Lichtfouse, M. Padervand, C. Wang, Visible–light–driven photocatalytic degradation of ciprofloxacin antibiotic by novel heterostructured coal fly ash waste:

Mechanism insight, toxicity pathway and DFT calculation, Mater. Today Chem. 42 (2024) 102388. https://doi.org/10.1016/j.mtchem.2024.102388.

[83] L. Qin, H. Ye, C. Lai, S. Liu, X. Zhou, F. Qin, D. Ma, B. Long, Y. Sun, L. Tang, M. Yan, W. Chen, W. Chen, L. Xiang, Citrate-regulated synthesis of hydrotalcite-like compounds as peroxymonosulfate activator - Investigation of oxygen vacancies and degradation pathways by combining DFT, Appl. Catal. B Environ. 317 (2022) 121704. https://doi.org/10.1016/j.apcatb.2022.121704.

[84] M. Yao, Y. Liu, L. Zhang, J. Wang, C. Xu, T. Qian, X. Liu, Synergistic adsorption and photodegradation of ciprofloxacin in water by biochar-supported titanates: Mechanistic analysis, DFT calculations and toxicity risk assessment, J. Water Process Eng. 70 (2025) 106964. https://doi.org/10.1016/j.jwpe.2025.106964.

[85] P. Gutiérrez-Sánchez, A. Hrichi, J.M. Garrido-Zoido, S. Álvarez-Torrellas, M. Larriba, M. Victoria Gil, H. Ben Amor, J. García, Natural clays as adsorbents for the efficient removal of antibiotic ciprofloxacin from wastewaters: Experimental and theoretical studies using DFT method, J. Ind. Eng. Chem. 134 (2024) 137–151. https://doi.org/10.1016/j.jiec.2023.12.044.

[86] C. Li, H. Lin, A. Armutlulu, R. Xie, Y. Zhang, X. Meng, Hydroxylamine-assisted catalytic degradation of ciprofloxacin in ferrate/persulfate system, Chem. Eng. J. 360 (2019) 612–620. https://doi.org/10.1016/j.cej.2018.11.218.

[87] D. Zheng, J. Zou, H. Xu, M. Wu, Y. Wang, C. Feng, E. Zheng, T. Wang, Y. Shi, Y. Chen, B. Li, Efficiency and mechanism of the degradation of ciprofloxacin by the oxidation of peroxymonosulfate under the catalysis of a Fe3O4/N co-doped sludge biochar, Chemosphere 325 (2023) 138387. https://doi.org/10.1016/j.chemosphere.2023.138387.

[88] Y. Ma, T. Lu, L. Yang, L. Wu, P. Li, J. Tang, Y. Chen, F. Gao, S. Cui, X. Qi, Z. Zhang, Efficient adsorptive removal of fluoroquinolone antibiotics from water by alkali and bimetallic salts co-hydrothermally modified sludge biochar, Environ. Pollut. 298 (2022) 118833. https://doi.org/10.1016/j.envpol.2022.118833.

[89] Y. Xiang, X. Yang, Z. Xu, W. Hu, Y. Zhou, Z. Wan, Y. Yang, Y. Wei, J. Yang, D.C.W. Tsang, Fabrication of sustainable manganese ferrite modified biochar from vinasse for enhanced adsorption of fluoroquinolone antibiotics: Effects and mechanisms, Sci. Total Environ. 709 (2020) 136079. https://doi.org/10.1016/j.scitotenv.2019.136079.

[90] Z.U. Zango, A. Garba, A. Haruna, S.S. Imam, A.U. Katsina, A.F. Ali, A.Z. Abidin, M.U. Zango, Z.N. Garba, A. Hosseini-Bandegharaei, A.U. Yuguda, H. Adamu, A systematic review on applications of biochar and activated carbon derived from biomass as adsorbents for sustainable remediation of antibiotics from pharmaceutical wastewater, J. Water Process Eng. 67 (2024) 106186. https://doi.org/10.1016/j.jwpe.2024.106186.

CRediT statements

Kawtar Ezzahi: Methodology , Writing - Original Draft

Imad Rabichi : Methodology , Writing - Original Draft

Hasna Befenzi : Methodology , Writing - Original Draft

Eric Record : Investigation

Taoufiq Bouzid : Software

Abdelghani Yaacoubi : Visualization

Abdelaziz Baçaoui : Investigation

Youssef Habibi : Investigation

Loubna El Fels : Conceptualization, Methodology, Supervision, Writing - Review & Editing